HHS Public Access

Author manuscript

Dev Cell. Author manuscript; available in PMC 2024 April 24.

Published in final edited form as:

Dev Cell. 2023 April 24; 58(8): 635–644.e4. doi:10.1016/j.devcel.2023.03.005.

Formation and function of the meningeal arachnoid barrier around the developing mouse brain

Julia Derk[1], **Christina N. Como**[1,2], **Hannah E. Jones**[1,3], **Luke R. Joyce**[4], **Sol Kim**[1,3], **Brady L. Spencer**[4], **Stephanie Bonney**[1,5], **Rebecca O'Rourke**[1], **Brad Pawlikowski**[1], **Kelly S. Doran**[4], **Julie A. Siegenthaler**[1,2,3,#,†]

[1]University of Colorado Anschutz Medical Campus, Department of Pediatrics, Section of Developmental Biology, Aurora, CO 80045

[2]University of Colorado Anschutz Medical Campus, Neuroscience Graduate Program, Aurora, CO 80045

[3]University of Colorado Anschutz Medical Campus, Cell Biology Stem Cells and Development Graduate Program, Aurora, CO 80045

[4]University of Colorado Anschutz Medical Campus, Department of Immunology and Microbiology, Aurora, CO 80045

[5]Current institution: Seattle Children's Research Institute, Seattle, WA.

Summary

The arachnoid barrier, a component of the blood-cerebrospinal fluid barrier (B-CSFB) in the meninges, is composed of epithelial-like, tight junction expressing cells. Unlike other central nervous system (CNS) barriers, developmental mechanisms and timing are largely unknown. Here we show that mouse arachnoid barrier cell specification requires repression of Wnt-β-catenin signaling and constitutively active β-catenin can prevent its formation. We also show the arachnoid barrier is functional prenatally and, in its absence, a small molecular weight tracer and the bacterium Group B *Streptococcus* can cross into the CNS following peripheral injection. Acquisition of barrier properties prenatally coincides with junctional localization of Claudin 11, and increased E-cadherin and maturation continues after birth, where postnatal expansion is marked by proliferation and re-organization of junctional domains. This work identifies

[#]Corresponding Author: Julie Siegenthaler, PhD, Associate Professor, University of Colorado, Anschutz Medical Campus, Dept of Pediatrics, Section of Developmental Biology, 12800 East 19th Ave, MS-8313 Aurora, CO 80045, Julie.Siegenthaler@cuanschutz.edu.

[†]Lead Contact

Author Contributions

The authors confirm contribution to the paper as follows: study conception and design: J.A.S, J.D., and B.P., data collection: J.D., C.N.C., H.E.J., L.R.J., S.K., B.L.S., S.B., J.A.S.; analysis and interpretation of results: J.D., C.N.C., H.E.J., L.R.J., S.K., B.L.S., S.B., R.O.R., B.P., K.D., J.A.S. ; draft manuscript preparation: J.D. and J.A.S. All authors reviewed the results and approved the final version of the manuscript.

Declaration of Interests

The authors have nothing to declare.

fundamental mechanisms that drive arachnoid barrier formation, highlights arachnoid barrier fetal functions, and provides novel tools for future studies on CNS barrier development.

eTOC

Derk et al. report the arachnoid barrier layer, a CNS barrier in the meninges, forms in the prenatal brain and is functional before birth to restrict peripheral tracers and bacteria. They show Wnt-β signaling suppression underlies arachnoid barrier cell specification and increased tight junction protein localization coincides with barrier functionality.

Graphical Abstract

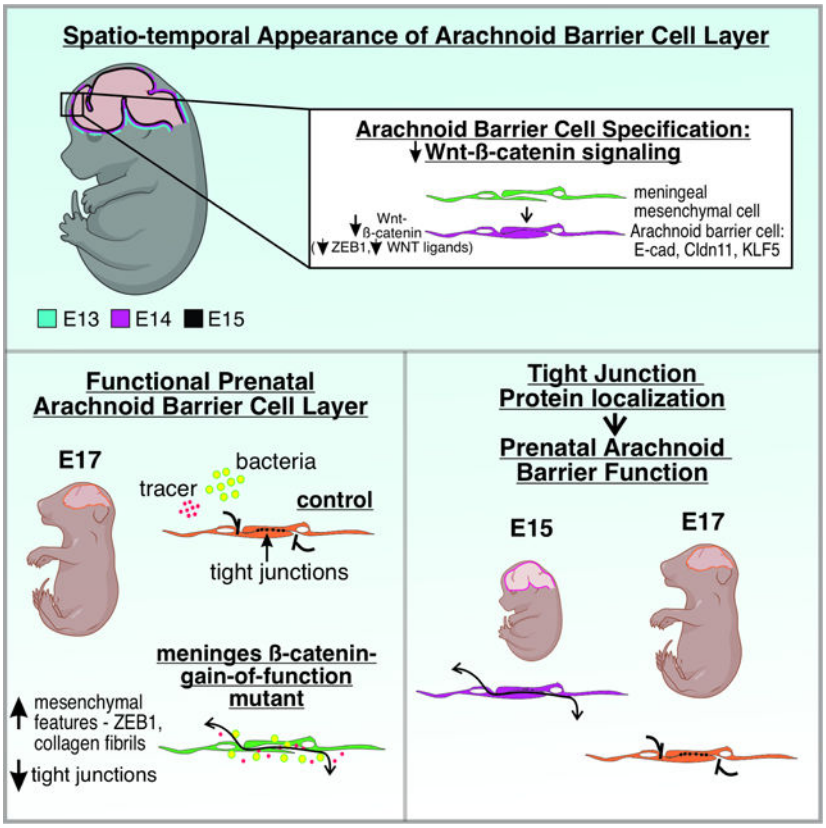

Introduction

The meningeal arachnoid barrier is a component of the blood-cerebrospinal fluid barrier (B-CSFB), that along with barriers at the pial vasculature and choroid plexus, regulates the free movement of molecules and cells into and out of the CSF filled subarachnoid space and ventricles[1–5]. Identifying mechanisms that drive blood-brain barrier (BBB) and B-CSFB develop is important, as their disruptions contribute to the pathophysiology of brain injury, neurodegenerative disorders, neuroinflammatory diseases, cancer, and the aged brain[6–11]. The arachnoid barrier separates the fenestrated blood vessels of the dura from the immune privileged CSF and is composed of epithelial-like cells connected by tight and adherens junctions[12–15]. Our prior work showed that in mouse meninges, arachnoid barrier

cells originate from mesenchymal precursor cells, similar to other meningeal fibroblasts at E12, but begin to express epithelial (E-cadherin) and tight junction (Claudin 11) proteins at around E14[16]. Similar transitions are also seen in the human and rat fetal brain[12]. Here we define developmental mechanisms that drive meningeal mesenchymal precursor cells to transition into epithelial-like arachnoid barrier cells with junctional properties around the CNS. We show that downregulation of Wnt signaling is a key mechanism underlying arachnoid barrier cell specification and that the barrier is functional as early as E17 to prevent passage of peripheral molecules into the CNS and foreign pathogens into the meninges. These studies significantly advance our knowledge on CNS barrier development and generates new tools and mechanistic insights that may empower future studies to uncover how the B-CSFB, and specifically the arachnoid barrier, contributes to CNS health and disease.

Results

At E14 arachnoid barrier cell specification is underway but incomplete, as arachnoid barrier cells (marked by E-cadherin expression) are present in the ventral forebrain meninges but are discontinuous in the dorsal forebrain meninges[16]. To compare the transcriptional signature of more mature arachnoid barrier cells to those that are likely actively specifying, we took our previously generated E14 mouse forebrain meningeal single cell transcriptome dataset[16] and analyzed clusters expression some *Cdh1* (E-cadherin), which in the meninges is only expressed by arachnoid barrier cells. The analysis identified three subclusters at different putative stages of arachnoid barrier development that we annotated as “Mature AB”, “PreAB1”, and “PreAB2” (Fig. 1A, B). Cells in the Mature AB subcluster had the highest expression of E-cadherin (*Cdh1*), Claudin 11 (*Cldn11*), and Klf5 (*Klf5*) (Fig. 1B). Pseudotime analysis using Slingshot[17] identified a distinct hierarchical lineage relationship among the three subclusters (Fig. 1A) and an Ingenuity Pathway Analysis (IPA) identified Wnt-β-catenin signaling as significantly down regulated in the cells of the Mature AB subcluster compared to both PreAB clusters ($\log10^{-3}$ adjusted P-value) (Fig. 1C). Specifically, cells in the Mature AB cluster had higher expression of *Cdh1* and Wnt inhibitor *Dkk2*, lower expression of Wnt target genes *Ccnd1* and *Jun* and Wnt ligands *Wnt6* and *Wnt5b* as compared to PreAB clusters. Of note, PreAB clusters expressed *Wnt6*, *Wnt5a*, *Wnt5b*, and *Wnt4* and Wnt target genes *Lef1* and *Zeb1*[18,19] (Fig. 1D). Zeb1 is a transcription factor that directly suppresses *Cdh1*gene activity[20,21] and *Zeb1* was nearly absent in the Mature AB cluster (Fig. 1D). The dura cluster, a cell layer anatomically located immediately above the arachnoid barrier layer, were enriched for Wnt inhibitors *Dkk2, Sfrp2,* and *Sfrp1 and* Wnt receptors *Fzd2* and *Fzd1*. These analyses of gene expression data suggested differentiation of arachnoid barrier cells from meningeal mesenchymal precursor cells requires decreased Wnt-β-catenin signaling.

To test the role of Wnt-β-catenin signaling in arachnoid barrier cell specification, we generated mouse mutants to constitutively elevate Wnt-β-catenin signaling in meningeal mesenchymal cells prior to arachnoid barrier cell specification. We crossed mice with *Tbx18-CreERT2* allele, which we previously showed drives Cre expression in all meningeal mesenchymal cells to mice with a floxed β-catenin gain of function allele (*Ctnnb1*-ex3-flox[22]) that upon Cre recombination, generates a constitutive active version of β-catenin

and a Cre reporter allele (*Ai14-flox*) that drives tdTomato expression (Fig. 1E). When we exposed pregnant mice to tamoxifen at E11 and E12, a time point prior to arachnoid barrier cell specification[16] and collected control tissue at E15 we observed E-cadherin+ arachnoid barrier cells were present in a continuous layer that covers the entire ventral to dorsal surfaces of the forebrain (Supp. Fig. 1A, B). Cre induced tdTomato expression in E-cadherin+ arachnoid barrier cells was ~90% expression in dorsal arachnoid barrier cells and ~50% expression in ventral arachnoid barrier cells (Supp. Fig. 1C), thus we were careful to make distinctions between these two areas in subsequent analysis.

Comparative analysis of the meninges in control and *Tbx18-CreERT2; Ctnnb1*-ex3-flox/+; *Ai14 flox/+* embryos (referred to as meningeal β-catenin-GOF, abbreviated mβ-cat-GOF) showed that E-cadherin+, Claudin11+, and nuclear Klf5+ arachnoid barrier cells were nearly absent from the mβ-cat-GOF E15 and E17 dorsal forebrain meninges (Fig. 1F, H, Ii, and Supp. Fig. 2A, 2B), demonstrating substantial regional failure of arachnoid barrier cell development in mβ-cat-GOF mutants. mβ-cat-GOF mutants had increased expression of direct Wnt-β-catenin target Lef1 in tdTomato+ cells (Fig. 1F, Iii), confirming elevated Wnt signaling in recombined cells. Meningeal fibroblasts in the expression of other pia, arachnoid, and dura cell layer markers were not altered and neocortical neuron layering and cell number appeared normal in mβ-cat-GOF mutants (Supp. Fig. 1E, Supp. Fig. 2C–E). Electron microscopy (EM) on E17 meninges of control and mβ-cat-GOF mutants highlighted multiple abnormalities in the mutant, including prominent gaps between cells, absence of tight junctions, and increased collagen deposition between cells located where the arachnoid barrier layer would normally be present in the control (Fig. 1G, Supp. Fig. 1D). This supports that in mβ-cat-GOF mutants, cells retain mesenchymal features and failed to differentiate into epithelial-like cells. Consistent with mesenchymal characteristics, E15 mβ-cat-GOF mutants had significantly more tdTomato+ cells expressing Zeb1, a mesenchymal transcription factor and Wnt-β-catenin transcriptional target (Fig. 1H, Iiii), most notably in the region where the arachnoid barrier cell layer (~6.5–10 μm above the brain surface) is observed in E15 control. Collectively these data point to a potential model of arachnoid barrier development where decreased Wnt-β-catenin signaling in meningeal mesenchymal cells, possibly due to reduced Wnt ligand expression and high Wnt inhibitors expression from the overlying dura, results in reduced Zeb1, increased E-cadherin expression, and acquisition of epithelial-like characteristics (Fig. 1J).

To investigate functional properties of the fetal arachnoid barrier, we tested the CNS permeability of E17 control and mβ-cat-GOF mutants to a small molecular weight fluorescent tracer (Biocytin-TMR, 893 Daltons) (Fig. 2A). Ten minutes after liver injection of Biocytin-TMR, we collected whole heads, sectioned, and visualized via microscopy. In controls, Biocytin-TMR signal was present in the dura, above the arachnoid barrier cell layer, but was excluded from the lower leptomeninges (arachnoid and pia) and brain below the intact arachnoid barrier (Fig 2B–D, G, H). In contrast, in dorsal forebrain regions where mβ-cat-GOF mutants lack an arachnoid barrier layer, Biocytin-TMR signal was present in the lower leptomeninges and in the superficial brain region directly below the meninges (Fig. 2B–D, G, H). Biocytin-TMR signal was absent in the deeper subventricular zone away from the brain surface in control or mutant mice (Fig. 2B, E, F), supporting that the BBB is not impaired in mβ-cat-GOF mutants. However since *Tbx18-CreERT2* recombines mural

cells (vascular smooth muscle cells and pericytes) that are required for BBB integrity[23,24], we analyzed Desmin+ mural cell in the meninges and the neocortex. Mural cell density associated with blood vessels in both regions were unaltered in mβ-cat-GOF mutants (Supp. Fig. 3A, B). Wnt-β-catenin signaling, a major pathway regulating BBB barrier properties, target Lef1 was highly expressed in control and mβ-cat-GOF leptomeninges and neocortex blood vasculature, but not in non-barrier dura vasculature (Supp. Fig 3C), showing additional evidence for an intact BBB properties in mβ-cat-GOF mutants. Collectively, the Biocytin-TMR analyses shows that the arachnoid barrier is functional by E17 and the lack of an arachnoid barrier in mβ-cat-GOF mutants permits access of peripheral molecules into the fetal leptomeninges and brain.

We next compared the ability of the bacterium, *Group B Streptococcus* (GBS), a pathogen that drives meningitis in neonates, to traverse into the leptomeninges following liver inoculation in control and mβ-cat-GOF mutants. We injected 10^6 Colony Forming Units (C.F.U.) of GFP-labeled GBS (~1 μm in diameter) bacteria into the livers of E17 animals and collected tissue 45 min later (Fig. 2A). In control animals, the amount of GFP-GBS+ in the leptomeninges was sparse, consistent with a functional arachnoid barrier, but the GBS burden was significantly higher in the leptomeninges of mβ-cat-GOF mutants leptomeninges (Fig. 2I, J). This indicates that the lack of an arachnoid barrier in mβ-cat-GOF mutants permits increased access for GBS to enter the prenatal meninges. Increased access of the GFP+ GBS biological tracer could not be attributed to alterations in the number of meningeal macrophages as there were equal numbers of IBA1+ cells in the meninges of control and mβ-cat-GOF mutant mice at baseline and 45 minutes after injection of GBS (Fig. 2K, L). There were no major differences in GBS burden in skin (Supp. Fig. 3E) indicating that distribution of systemic GBS was not overtly altered between groups. We detected $CD11b^+$, $F4/80^+$ monocytes/macrophages and $CD11b^+$, $Ly6G^+$ neutrophils in blood and fetal livers of control and mβ-cat-GOF mutants (Supp. Fig. 3F, G) supporting there is no obvious impairments in the innate immune system that could potentially underlie observed differences in meningeal GBS of controls and mβ-cat-GOF mutants.

To investigate the maturation of the arachnoid barrier, we documented the temporal and spatial appearance of E-Cadherin/Claudin 11 co-expressing arachnoid barrier cells in the prenatal meninges and identified the earliest age when the arachnoid barrier can functionally restrict the passage of a small molecule treace. At E12, E-cadherin/Claudin 11 double positive arachnoid barrier cells are not detectable in the meninges (Fig 3A, B). A few cells are expressing cytosolic Claudin 11 at E12 in/near the brain, but these cells did not co-express E-cadherin, indicative of another cell type (Fig. 3A, B). At E13 we observed consistent E-cadherin and Claudin 11 double-positive cells forming a layer in the ventral hindbrain with a patchy layer of a double-positive cells in the ventral forebrain, but very few double positive cells in the dorsal forebrain (Fig. 3A, B). At E14, E-cadherin/Claudin 11 double-positive cells were more numerous in the dorsal forebrain (Fig. 3A. B) but did not form a continuous layer in this region until E15 (Supp. Fig. 1A, B). Biocytin-TMR tracer and plate reader analysis showed that the superficial cortex of E15 brains had significantly more tracer signal than the superficial cortices from E17, postnatal, and adult animals (Fig. 3C). This indicates that the E15 arachnoid barrier layer in the dorsal forebrain is ‘leaky”, despite the presence of a continuous E-cadherin/Claudin 11 double-positive cell

layer. Analysis of tissue sections supported these findings showing that the amount of tracer below the arachnoid barrier in the leptomeninges was significantly higher at E15 compared to E16 and E17 meninges (Fig. 3D, E). These analyses demonstrate that the arachnoid barrier cellular layer starts to form around the brain at E13 and is continuous by E15, and that functional restriction to small molecular weight tracers does not occur until slightly later.

We next analyzed localization of tight and adherens junction proteins between arachnoid barrier cells in pre-, postnatal and adult mice, as barrier integrity critically depends on cell-cell junctions. Consistent with previous electron microscopy and freeze fracture studies[3,13], adult cerebral leptomeninges whole mounts show arachnoid barrier cells are connected by tight and adherens junctions marked by co-localization of E-cadherin, Claudin 11, and ZO-1 proteins in high expression areas between cells (Supp. Fig. 4A), a pattern that matches freeze fracture studies describing tight junction strands in the arachnoid barrier layer of rodents[13,14]. To identify when junctions appear between arachnoid barrier cells and how junctional protein localization change with age, we immunolabeled cerebral leptomeninges wholemounts and measured junctional protein localization (junctional vs. non-junctional) and junctional density at E15, E17, P4, P7 and adults[25,26] (Fig. 4A, B, H-J). At E15, when the arachnoid barrier layer does not restrict small molecule tracers, Claudin 11 protein expression was diffuse and mostly non-junctional (Fig. 4A) with fewer Claudin 11+ junctions compared to E-cadherin junctions (Fig. 4B, C). E15 E-cadherin junctions, though more abundant than Claudin 11 junctions, had lower junctional fluorescence intensity compared to later time points (Fig. 4A, B, H, J, and K). At E17, the number of Claudin 11+ and E-cadherin+ junctions had increased and were at equal numbers (Fig. 4A–C). EM of E15 and E17 meninges showed that although the overall layering and cellular composition of the meninges between the two timepoints was similar, including similar organization of arachnoid barrier cell processes, many more electron dense tight junctions were present at E17 as compared to E15 (Fig. 4D–G, Supp. Fig. 4B). We also observed from pre- to postnatal time points, there was a decrease in non-junctional expression of Claudin 11 (Fig. 4A, I) and to a lesser extent non-junctional E-cadherin (Fig. 4A, J). Finally, arachnoid barrier cells are connected by junctions on multiple sides, creating domains (Fig. 4L). We observe that arachnoid barrier domain area increased from E17 to P7 and adult time points (Fig. 4A, L, and M). Arachnoid barrier cell proliferation measured by EdU pulse-labeling was initially high at E17, decreased between P4 and P7 and is absent in the adult (Supp. Fig. 4C, D), indicative of a concomitant decrease in proliferation as domain size increases during brain growth. This analysis shows that the arachnoid barrier maturation continues into postnatal ages and its ability to act as a selective barrier coincides with the increased junctional expression of Claudin 11 and E-Cadherin, along with increased density of tight junctions at E17.

Taken together, a model of arachnoid barrier layer development emerges from our data. First, the arachnoid barrier cell layer arises from meningeal mesenchymal precursors in a temporally and spatially restricted manner from E13 to E15 through a mechanism involving downregulation of Wnt-β-catenin. In the cerebral leptomeninges, E-cadherin forms adherens junctions between arachnoid barrier cells by E15, followed by junctional Claudin 11 and a functional barrier by E17. To accommodate brain surface area growth from prenatal to

adult stages, the arachnoid barrier cells proliferate in pre- and early postnatal stages, but later arachnoid barrier domain areas increase to expand the arachnoid barrier layer while maintaining a functional barrier (Fig. 4N).

Discussion

The importance of arachnoid barrier in adult B-CSFB function is supported by several structural and tracer studies[2,3,13,14] and recent work showing meningeal barrier leakage caused by absence of a meningeal T cell subtype resulting in microglia activation and cognitive deficits[27]. Far less is known about when arachnoid barrier cells specify and when it forms functional layer. This study provides fundamental insights into arachnoid barrier formation, describing arachnoid barrier cells from their first emergence at E13, to their expression of tight junctions and barrier properties by E17, through their postnatal maturation as and expansion around the growing mouse brain. This process of arachnoid barrier maturation resembles prenatal emergence and postnatal maturation of the BBB, with key differences. The arachnoid barrier becomes functional just after the BBB which is restrictive to tracers by E13-E14, depending on brain region[28]. Arachnoid barrier cells are also specified *de novo* from meningeal mesenchymal cells, dependent on downregulation of Wnt-β-catenin signaling. This downregulation of Wnt-β-catenin signaling is in contrast to BBB vasculature which grows into the CNS via angiogenesis of existing vasculature surrounding the CNS and acquires barrier properties via upregulation of Wnt−β-catenin signaling, induced by locally produced Wnt ligands. Future work will expand upon the current approaches detailed here to determine if there is a gradual spatial-temporal "tightening" that [28–30], or if it is an "all-or-none" phenomenon. These experiments, in conjunction with immuno-gold labeling with electron microscopy and super-resolution imaging of Claudin 11 and E-cadherin, will be important to better define specific junction protein localization and functions at subcellular resolution.

Our work here shows that the arachnoid barrier can prevent the passage of peripherally injected dyes or bacteria in the fetal CNS as early as E17, which suggests a potentially important protective function for the prenatal arachnoid barrier. Our work also shows that arachnoid barrier continues to mature throughout postnatal life, a time when it must also expand in size to match brain and skull growth. We also show that this postnatal expansion is facilitated by an increase in the junctional domain size, a mechanism potentially conducive to the maintenance of an already established barrier. The arachnoid barrier postnatal maturation is also interesting in the context of meningitis as neonates are uniquely susceptible to GBS induced bacterial meningitis[31–33]. Our findings suggest that the still maturing postnatal arachnoid barrier could contribute to this neonatal vulnerability. In support of this idea, recent work showed that the neonatal choroid plexus has increased permeability to bacterial crossing, due to immature cell-cell junctions, and this contributes to neonatal susceptibility in bacterial meningitis[34].

Our work here also provides several new tools that can be used to investigate CNS barrier development. These include our prenatal model of defective arachnoid barrier development, whole mounts to visualize arachnoid barrier layer junctional organization, and functional assays that may aid in studies to address outstanding questions about the

arachnoid barrier. There remains much unknown on the basic biology of the arachnoid barrier, such as: how does Wnt-β-catenin signaling suppression support arachnoid barrier cell specification and how are E-cadherin and Claudin 11 localized to cell-cell junctions in newly specified arachnoid barrier cells to form a functional structure? Disease relevant questions include how the immature or mature arachnoid barrier responds to acute physical injury vs. infectious agents vs. chronic disease, and if the arachnoid barrier can reactivate developmental programs to allow for regeneration.

Limitations of the Study

This study is focused primarily on prenatal barrier function due to the early postnatal lethality of mβ-cat-GOF mutants. Given that there is extensive postnatal maturation of the meninges to acquire new functional properties, including diversification and maturation of meningeal immune populations[35], development and function of dural lymphatics[36–38], and the emergence of glymphatic flow[39], there are numerous future directions to explore as we continue to investigate the potential contributions of the arachnoid barrier to CNS health and diseases, particularly in meningitis. In this study, our analysis of GBS infection only serves as a 'biological tracer', not an investigation of meningitis pathogenesis. Thus, future studies looking at CNS and meningeal inflammatory responses, long-term implications, and mechanisms of GBS infiltration in postnatal and adult animals, including those with arachnoid barrier impairment, will be critical for identifying the functional role(s) and response(s) of the arachnoid barrier during meningitis and will pave the road to further understanding how the arachnoid barrier may participate in a variety of diseases.

STAR Methods

RESOURCE AVAILABILITY

Lead contact—Further information and requests for resources and reagents should be directed to and will be fulfilled by the Lead Contact, Julie Siegenthaler (julie.siegenthaler@cuanschutz.edu).

Materials Availability—This study did not generate new unique materials.

Data and Code Availability—All data to support the findings of this study are included in this paper and the supplemental information. Any additional information required to reanalyze the data reported in this paper are available from the lead contact upon reasonable request.

EXPERIMENTAL MODEL AND SUBJECT DETAILS

Animals.—Mice used for experiments here were housed in specific-pathogen-free facilities approved by the AALAC and all experiments were performed in accordance with protocols approved by the University of Colorado Anschutz Medical Campus IACUC committee. The following mouse strains were used in this study: 1) Tbx18$^{tm3.1(cre/ERT2)Sev/J}$ (Jackson Laboratory Stock No: 031520; RRID: IMSR_JAX:031520), 2) Ai14fl/fl (Gt(ROSA)26Sor$^{tm14(CAG-tdTomato)Hze,}$ Jackson Laboratory Stock No: 007914 RRID: IMSR_JAX:007914), 3) *Ctnnb1*$^{lox(ex3)}$ and 4) C57Blk/6J (Jackson: 000664) wildtype

animals were bred to generate embryonic or postnatal litters (E12, E13, E15, E17, P4, P7) or collected as adults (12 weeks) for wholemounts analysis. For timed pregnancy, males and females were placed together on the afternoon and presence of a plugged was checked AM daily; the day the plug was detected was counted as embryonic day 0.

To activate Cre-mediated recombinase activity, pregnant dams were injected intraperitoneally with 100 μl of tamoxifen (Sigma, Cat#: T5648) dissolved in corn oil (Sigma cat#: C8267; 20 mg/ml) at embryonic day 11 and 12. To measure arachnoid barrier tracer leakage, E15, E16 or E17 fetal mice were injected in liver with 2 μl of 0.25% Biocytin-TMR (Thermo Fisher) for 10 min, perfused intracardiac with PBS to remove blood that contains tracer and isolated tissue was used for immunohistochemistry or plate reader analysis (protocol adapted from the Gu Laboratory for BBB analysis[28]). Postnatal and adult mice were injected intraperitoneally 30 min prior to perfusion and isolation of tissue, postnatal mice were injected with 25 μl of 0.25% Biocytin-TMR and adult mice were injected with 100 μl of 0.25% Biocytin-TMR. For GBS inoculation, mice were injected in the liver with ~1.2×10^6 CFU and sacrificed 45 min later for isolation of tissues. For EdU detection, we administered EdU (2.5 mg/mL) via intraperitoneal injection prior to anesthetization (embryonic: 150 μL into pregnant dam, P0-P21: 50 μL, adult: 100 μL) and allowed to circulate for 2 h prior to anesthetization.

Bacterial Culture—*Streptococcus agalactiae*, (Group B *Streptococcus*, GBS) strain COH1+pDESTerm-GFP, has been described previously described[40] grown statically overnight at 37˚C in Todd-Hewitt Broth supplemented with 5 μg/mL erythromycin. Bacteria were sub-cultured and grown to mid-exponential phase before resuspension in PBS.

METHODS DETAILS

Bioinformatic Analysis of Single Cell Data.—R Studio with R version 3.6.3 and Seurat V.4 were used for further analysis of our previously published dataset (DeSisto et al., *Developmental Cell*, 2020)[16]. All clusters that contained arachnoid barrier cells, as defined by *Cdh1* at >1 expression, were subsetted out and subclustered using FindNeighbors(reduction='pca', dims=1:30) and FindClusters(resolution=0.5). Slingshot pseudotime lineage analysis was applied to the new subclusters to determine the lineage pathway from immature to mature arachnoid barrier cells[16]. Subsequently, Ingenuity Pathway Analysis (Qiagen) was applied to lists of differentially expressed genes between each cluster to determine putative upstream and master regulators of the changes seen across the trajectory.

Immunohistochemistry of Whole Head Sections—Embryos were collected and whole heads fixed for 48h with 4% paraformaldehyde followed by 20% sucrose and frozen in OCT compound (Tissue-Tek). Tissue was cryosectioned in 12μm increments and tissue-mounted slides were subjected to antigen retrieval by immersing the slides in solution of 0.01M citric acid, 0.05% Tween, pH 6, and heating in a pressure cooker (Cuisinart Model CPC-600) for 6 min. No antigen retrieval was performed when staining for Claudin11, Desmin, Klf5, Ctip2, GFP, or E-cadherin. The tissue was permeabilized by incubating for 10 min at room temperature in PBS with 0.1% Triton-X (Sigma), blocked in 2% lamb

serum/0.05% Triton-X solution for 40 min at room temperature and primary and secondary solution was 0.05% Triton-X in PBS. Incubation in the following primary antibodies was conducted overnight at 4°C in appropriate solution: rabbit anti-S100A6 (1:100; Novus NBP2–44492), mouse anti-CRABP2 (1:100 Millipore; MAB5488), rabbit anti-RALDH2 (1:100, Sigma-Aldrich HPA010022), chicken anti-GFP (1:500, Invitrogen A10262), mouse anti-E-cadherin (1:100, BD Transduction Laboratories 610181), rabbit anti-Desmin (1:100, Cell Signaling (5332S), rabbit anti-Lef1 (1:100, Cell Signaling 2230S, rabbit anti-Claudin 11 (1:100, Thermo Fisher, PIPA568608), chicken anti-GFP (1:200; Rockland), rat anti-Ctip2 [25B6] (1:200, Abcam, ab18465) and rabbit anti-Klf5 (1:100, Genetex, GTX103289). Following incubation with primary antibodies, tissue sections were incubated for 60 min with appropriate Alexafluor-conjugated secondary antibodies (Invitrogen) and DAPI (1:1000; Invitrogen), washed in PBS and then coverslipped using Fluoromount-G (Southern Biotech). Slides were allowed to dry overnight at room temperature and then imaged or stored at −20 degree C until imaging.

Whole Mount Preparations and Immunohistochemistry—All whole mount dissection and immunostaining and EdU detection in whole mount are detailed at length in our protocol paper Jones et al., 2022 *Neurophotonics*[26].

Microscopy Imaging and Image Quantification—Confocal images were obtained using a Zeiss 780 Laser Scanning Microscope with associated Zeiss Zen Black software. Images were processed in FIJI Image J and Graphic software. For cell counts in Fig. 1, images were subjected to thresholding and the number of positive cells were counted per 100 μm of leptomeninges was counted (or 100 μm of E-cadherin+ cells, if listed). For Fig. 2D and 2F, a 15 μm line was drawn in FIJI within 20 μm of the cortical surface (Fig. 2D) or where nuclei patterns in DAPI indicated the subventricular zone of the mouse brain (Fig. 2F) and the average intensity across that line was recorded for each sample. For Fig. 2H, 5 control E17 animals with Claudin 11 staining were used to determine the average thickness of the arachnoid barrier (~1.7 μm) and the distance from the outer surface of the arachnoid barrier to the pial/brain surface (~8 μm). Subsequently, a line from the pial/brain surface was extended up for 8 μm for both control and mutant animals and the biocytin intensity was plotted spatially. For Fig. 2J, images were separated by color with the green (488 nm) channel subjected to thresholding, and a box of 8 μm (height of the arachnoid barrier) by 100 μm was drawn to count all GFP+ GBS (> 0.5 μm in diameter, as shown in Supp. Fig 3D). For Fig. 4D and 4E, a 6 μm line was drawn across the junctions (as depicted in 4B) and an intensity profile was plotted with the outer 2.5 μm indicating cytosolic portions of the cell and the middle peak indicating the junction. For Fig. 4M, the perimeter of cell domains was traced using the freehand tool in FIJI and the area within was measured for each sample. E15 were excluded from this analysis because it was not possible to determine a unique cellular domain at this age. For Supp. Fig 4D, Klf5 was used to mark arachnoid barrier nuclei and EdU+/Klf5+ nuclei were quantified as proliferating arachnoid barrier cells. Data are plotted as a percentage, quantified by the division of EdU and KLF5 double positive nuclei by all KLF5 positive nuclei * 100.

Flow cytometric analysis of immune cells in E17 blood and liver—Single cell suspensions were prepared from E17 blood by ACK lysis of red blood cells at room temperature. Cells were washed with RPMI 1640 (Gibco), pelleted at 300 x g for 5 minutes at 4 °C and resuspended in MACS buffer (1X PBS (pH 7.2) + 2mM EDTA + 0.5% BSA). Single cell suspensions were prepared from E17 livers by harvesting them, mincing with forceps, and incubating in 2% fetal bovine serum (Gibco) in PBS and 1mg/ml Collagenase type 4 (Worthington Biochemical) with 100U/ml Deoxyribonuclease 1 (Sigma) for 15 minutes at 37 degrees on a nutator. Red blood cells were removed by resuspending the pellet in red blood cell lysis buffer for 5 minutes at room temperature and washing with RPMI 1640 (Gibco). Cells were resuspended in MACS buffer and filtered through a 70 μm cell strainer.

Blood and liver single cell suspensions were first stained with eBioscience Fixable Viability Dye eFluor 506 (Catalog # 65–0866-18) in PBS for 30 minutes at room temperature. Cells were stained with the following anti-mouse surface antibodies in MACS buffer for 30 minutes at room temperature: from Biolegend—F4/80-BV785 (clone BM8; Catalog #123141), Ultra-LEAF Purified CD16/32 (clone 93; Catalog # 101330]; from BDBiosciences—CD45-BUV395 (clone 30-F11; Catalog # 564279); from Thermo Fisher Invitrogen—CD11b-FITC (clone M1/70; Catalog # 11–0112-41), Ly6G-APC (clone 1A8-Ly6g; Catalog # 17–9668-82).

After surface antibody staining, the cells were fixed (30 minutes at room temperature) using the FoxP3 fixation/permeabilization kit (Thermo Fisher Scientific, Catalog # 00–5523-00). Stained cells were analyzed on a BD LSRFortessa (BD Biosciences) using the BD FacsDiva software (v9). Data were analyzed with BD FlowJo software v 10.8.1.

Electron Microscopy—For electron microscopy experiments, E15 (n=2) and E17 (n=2) wildtype fetuses or E17 littermate control (n=1) and mβ-cat-GOF (n=1) fetuses were perfused intracardiac with 2.5 ml 4% paraformaldehyde and 1% glutaraldehyde in 0.1M cacodylate buffer (pH 7.4). Whole heads were removed, skin and lower jaw and any excess cranial facial tissue was removed with forceps, and whole heads were fixed overnight at 4 degree C in 2% paraformaldehyde and 2% glutaraldehyde in 0.1M cacodylate buffer (pH 7.4). Heads were embedded in 3% agarose (1:1 low-melt (Invitrogen Cat#: 16520–050) and genetic analysis grade (Fisher Scientific Cat#: PB1356–500)) in PBS sectioned at 100μm increments using a vibratome (Leica), collected in PBS and then stored in 2% paraformaldehyde and 2% glutaraldehyde in 0.1M cacodylate buffer (pH 7.4) until processing. Care was taken to select slices for EM in which the brain remained fully attached to cranial tissue to ensure the brain, meninges and calvarium remained intact through processing; any slices with slight detachment were not used for further processing. The tissue slices were rinsed in 100mM cacodylate buffer and then immersed in 1% osmium and 1.5% potassium ferrocyanide for 15min, rinsed five times in cacodylate buffer, immersed in 1% osmium for 1 hour, and then rinsed again five times for 2min each in cacodylate buffer and two times briefly in water. The tissue was then transferred to graded ethanol (50, 70, 90, and 100%) containing 2% uranyl acetate for 15 minutes each. Finally, it was transferred through propylene oxide at room temperature and then embedded in LX112 and cured for 48 h at 60°C in an oven. The blocks were trimmed to form a small trapezoid

that contained brain, meninges and calvarium and ultra-thin sections (65nm) were cut on a Reichert Ultracut E and were picked up on Formvar-coated slot grids (EMS). Sections were imaged on a FEI Tecnai G2 transmission electron microscope (Hillsboro, OR) with an AMT digital camera (Woburn, MA).

Quantification and Statistical Analysis—Statistical analyses were performed as described in the text using GraphPad Prism, where Two-Way ANOVAs and multiple comparisons with Tukey adjustments were performed in instances with two or more groups and Students' T-tests were performed to compare groups of two, after normality assumption was achieved. Information on statistical tests used and number of replicates (n) used for each experiment are listed in the figure legend or methods and all graphs report mean and standard deviation (SD), with the exception of Fig. 2H and 3D where the mean and standard error of the mean (SEM) are reported. In all experiments, n is the number of individual animals used for quantitative analyses (fetal, postnatal or adult).

Supplementary Material

Refer to Web version on PubMed Central for supplementary material.

Acknowledgements

This work was supported by R01 NS098273 to J.A.S. from NIH/NINDS, F32 NS122999 for J.D. from the NIH/NINDS, F32 AI143203 for B.L.S. from the NIH/NIAID, and R01NS116716 from the NIH/NINDS to K.S.D. We thank Dr. Anza Darehshouri from the Electron Microscopy Core Facility at the University of Colorado Anschutz Medical Campus for preparation of the samples for electron microscopy and help with imaging. Finally, we thank Mark Ostrander and the Developmental Biology Postdoctoral Program at the University of Colorado Anschutz Medical Campus for expert administrative and professional development support to J.D. throughout the completion of these studies.

Literature Cited

1. Roth TheodoreL., Nayak D., Atanasijevic T, Koretsky AlanP., Latour LawrenceL, and McGavern DorianB. (2013). Transcranial amelioration of inflammation and cell death after brain injury. Nature 505, 223–228. 10.1038/nature12808. [PubMed: 24317693]
2. Rodriguez-Peralta LA (1957). The role of the meningeal tissues in the hemato-encephalic barrier. J. Comp. Neurol 107, 455–473. 10.1002/cne.901070308. [PubMed: 13475509]
3. Balin BJ, Broadwell RD, Salcman M, and El-Kalliny M. (1986). Avenues for entry of peripherally administered protein to the central nervous system in mouse, rat, and squirrel monkey. J. Comp. Neurol 251, 260–280. 10.1002/cne.902510209. [PubMed: 3782501]
4. Ichikawa H, and Itoh K. (2011). Blood–arachnoid barrier disruption in experimental rat meningitis detected using gadolinium-enhancement ratio imaging. Brain Res. 1390, 142–149. 10.1016/j.brainres.2011.03.035. [PubMed: 21435335]
5. Ichikawa H, Ishikawa M, Fukunaga M, Ishikawa K, and Ishiyama H. (2010). Quantitative evaluation of blood–cerebrospinal fluid barrier permeability in the rat with experimental meningitis using magnetic resonance imaging. Brain Res. 1321, 125–132. 10.1016/j.brainres.2010.01.050. [PubMed: 20114032]
6. Liebner S, Dijkhuizen RM, Reiss Y, Plate KH, Agalliu D, and Constantin G. (2018). Functional morphology of the blood-brain barrier in health and disease. Acta Neuropathol. (Berl.) 135, 311–336. 10.1007/s00401-018-1815-1. [PubMed: 29411111]
7. Sweeney MD, Zhao Z, Montagne A, Nelson AR, and Zlokovic BV (2019). Blood-Brain Barrier: From Physiology to Disease and Back. Physiol. Rev 99, 21–78. 10.1152/physrev.00050.2017. [PubMed: 30280653]

8. Derk J, Jones HE, Como C, Pawlikowski B, and Siegenthaler J. (2021). Living on the edge of the CNS: meninges cell diversity in health and disease. Front. Cell. Neurosci. Accepted-In Press.
9. Alves de Lima K, Rustenhoven J, and Kipnis J. (2020). Meningeal Immunity and Its Function in Maintenance of the Central Nervous System in Health and Disease. Annu. Rev. Immunol 38, 597–620. 10.1146/annurev-immunol-102319-103410. [PubMed: 32340575]
10. Brkic M, Balusu S, Van Wonterghem E, Gorle N, Benilova I, Kremer A, Van Hove I, Moons L, De Strooper B, Kanazir S, et al. (2015). Amyloid Oligomers Disrupt Blood-CSF Barrier Integrity by Activating Matrix Metalloproteinases. J. Neurosci 35, 12766–12778. 10.1523/JNEUROSCI.0006-15.2015. [PubMed: 26377465]
11. Iliff JJ, Wang M, Liao Y, Plogg BA, Peng W, Gundersen GA, Benveniste H, Vates GE, Deane R, Goldman SA, et al. (2012). A paravascular pathway facilitates CSF flow through the brain parenchyma and the clearance of interstitial solutes, including amyloid β. Sci. Transl. Med 4, 147ra111. 10.1126/scitranslmed.3003748.
12. Uchida Y, Sumiya T, Tachikawa M, Yamakawa T, Murata S, Yagi Y, Sato K, Stephan A, Ito K, Ohtsuki S, et al. (2019). Involvement of Claudin-11 in Disruption of Blood-Brain, -Spinal Cord, and -Arachnoid Barriers in Multiple Sclerosis. Mol. Neurobiol 56, 2039–2056. 10.1007/s12035-018-1207-5. [PubMed: 29984400]
13. Nabeshima S, Reese TS, Landis DMD, and Brightman MW (1975). Junctions in the meninges and marginal glia. J. Comp. Neurol 164, 127–169. 10.1002/cne.901640202. [PubMed: 810497]
14. Rascher G, and Wolburg H. (1997). The tight junctions of the leptomeningeal blood-cerebrospinal fluid barrier during development. J. Hirnforsch 38, 525–540. [PubMed: 9476217]
15. Polanco J, Reyes-Vigil F, Weisberg SD, Dhimitruka I, and Brusés JL (2021). Differential Spatiotemporal Expression of Type I and Type II Cadherins Associated With the Segmentation of the Central Nervous System and Formation of Brain Nuclei in the Developing Mouse. Front. Mol. Neurosci 14, 25. 10.3389/fnmol.2021.633719.
16. DeSisto J, O'Rourke R, Jones HE, Pawlikowski B, Malek AD, Bonney S, Guimiot F, Jones KL, and Siegenthaler JA (2020). Single-Cell Transcriptomic Analyses of the Developing Meninges Reveal Meningeal Fibroblast Diversity and Function. Dev. Cell 54, 43–59.e4. 10.1016/j.devcel.2020.06.009. [PubMed: 32634398]
17. Street K, Risso D, Fletcher RB, Das D, Ngai J, Yosef N, Purdom E, and Dudoit S. (2018). Slingshot: cell lineage and pseudotime inference for single-cell transcriptomics. BMC Genomics 19, 477. 10.1186/s12864-018-4772-0. [PubMed: 29914354]
18. Sánchez-Tilló E, de Barrios O, Siles L, Cuatrecasas M, Castells A, and Postigo A. (2011). β-catenin/TCF4 complex induces the epithelial-to-mesenchymal transition (EMT)-activator ZEB1 to regulate tumor invasiveness. Proc. Natl. Acad. Sci. U. S. A 108, 19204–19209. 10.1073/pnas.1108977108. [PubMed: 22080605]
19. Sánchez-Tilló E, Fanlo L, Siles L, Montes-Moreno S, Moros A, Chiva-Blanch G, Estruch R, Martinez A, Colomer D, Győrffy B, et al. (2014). The EMT activator ZEB1 promotes tumor growth and determines differential response to chemotherapy in mantle cell lymphoma. Cell Death Differ. 21, 247–257. 10.1038/cdd.2013.123. [PubMed: 24013721]
20. Puisieux A, Brabletz T, and Caramel J. (2014). Oncogenic roles of EMT-inducing transcription factors. Nat. Cell Biol 16, 488–494. 10.1038/ncb2976. [PubMed: 24875735]
21. Liu Y, El-Naggar S, Darling DS, Higashi Y, and Dean DC (2008). Zeb1 links epithelial-mesenchymal transition and cellular senescence. Development 135, 579–588. 10.1242/dev.007047. [PubMed: 18192284]
22. Harada N, Tamai Y, Ishikawa T, Sauer B, Takaku K, Oshima M, and Taketo MM (1999). Intestinal polyposis in mice with a dominant stable mutation of the beta-catenin gene. EMBO J. 18, 5931–5942. 10.1093/emboj/18.21.5931. [PubMed: 10545105]
23. Daneman R, Zhou L, Kebede AA, and Barres BA (2010). Pericytes are required for blood–brain barrier integrity during embryogenesis. Nature 468, 562–566. 10.1038/nature09513. [PubMed: 20944625]
24. Armulik A, Genové G, Mäe M, Nisancioglu MH, Wallgard E, Niaudet C, He L, Norlin J, Lindblom P, Strittmatter K, et al. (2010). Pericytes regulate the blood–brain barrier. Nature 468, 557–561. 10.1038/nature09522. [PubMed: 20944627]

25. Bonney S, Seitz S, Ryan CA, Jones KL, Clarke P, Tyler KL, and Siegenthaler JA (2019). Gamma Interferon Alters Junctional Integrity via Rho Kinase, Resulting in Blood-Brain Barrier Leakage in Experimental Viral Encephalitis. mBio 10, e01675–19. 10.1128/mBio.01675-19. [PubMed: 31387911]
26. Jones Hannah E., Abrams Kelsey A., and Siegenthaler Julie A. (2022). Techniques for visualizing fibroblast-vessel interactions in the developing and adult CNS. Neurophotonics 9, 1–17. 10.1117/1.NPh.9.2.021911.
27. Zhang Y, Bailey JT, Xu E, Singh K, Lavaert M, Link VM, D'Souza S, Hafiz A, Cao J, Cao G, et al. (2022). Mucosal-associated invariant T cells restrict reactive oxidative damage and preserve meningeal barrier integrity and cognitive function. Nat. Immunol, 1–12. 10.1038/s41590-022-01349-1.
28. Ben-Zvi A, Lacoste B, Kur E, Andreone BJ, Mayshar Y, Yan H, and Gu C. (2014). MSFD2A is critical for the formation and function of the blood brain barrier. Nature 509, 507–511. 10.1038/nature13324. [PubMed: 24828040]
29. Sohet F, Lin C, Munji RN, Lee SY, Ruderisch N, Soung A, Arnold TD, Derugin N, Vexler ZS, Yen FT, et al. (2015). LSR/angulin-1 is a tricellular tight junction protein involved in blood–brain barrier formation. J. Cell Biol 208, 703–711. 10.1083/jcb.201410131. [PubMed: 25753034]
30. Sasson E, Anzi S, Bell B, Yakovian O, Zorsky M, Deutsch U, Engelhardt B, Sherman E, Vatine G, Dzikowski R, et al. (2021). Nano-scale architecture of blood-brain barrier tight-junctions. eLife 10, e63253. 10.7554/eLife.63253. [PubMed: 34951586]
31. Kurian NK, and Modi D. (2022). Mechanisms of group B Streptococcus-mediated preterm birth: lessons learnt from animal models. Reprod. Fertil 3, R109–R120. 10.1530/RAF-21-0105. [PubMed: 35794927]
32. Palackdkharry CS, Wottrich S, Dienes E, Bydon M, Steinmetz MP, and Traynelis VC (2022). The leptomeninges as a critical organ for normal CNS development and function: First patient and public involved systematic review of arachnoiditis (chronic meningitis). PloS One 17, e0274634. 10.1371/journal.pone.0274634.
33. Furuta A, Brokaw A, Manuel G, Dacanay M, Marcell L, Seepersaud R, Rajagopal L, and Adams Waldorf K. (2022). Bacterial and Host Determinants of Group B Streptococcal Infection of the Neonate and Infant. Front. Microbiol 13.
34. Travier L, Alonso M, Andronico A, Hafner L, Disson O, Lledo P-M, Cauchemez S, and Lecuit M. (2021). Neonatal susceptibility to meningitis results from the immaturity of epithelial barriers and gut microbiota. Cell Rep. 35, 109319. 10.1016/j.celrep.2021.109319. [PubMed: 34192531]
35. Van Hove H, Martens L, Scheyltjens I, De Vlaminck K, Pombo Antunes AR, De Prijck S, Vandamme N, De Schepper S, Van Isterdael G, Scott CL, et al. (2019). A single-cell atlas of mouse brain macrophages reveals unique transcriptional identities shaped by ontogeny and tissue environment. Nat. Neurosci 22, 1021–1035. 10.1038/s41593-019-0393-4. [PubMed: 31061494]
36. Antila S, Karaman S, Nurmi H, Airavaara M, Voutilainen MH, Mathivet T, Chilov D, Li Z, Koppinen T, Park J-H, et al. (2017). Development and plasticity of meningeal lymphatic vessels. J. Exp. Med 214, 3645–3667. 10.1084/jem.20170391. [PubMed: 29141865]
37. Aspelund A, Antila S, Proulx ST, Karlsen TV, Karaman S, Detmar M, Wiig H, and Alitalo K. (2015). A dural lymphatic vascular system that drains brain interstitial fluid and macromolecules. J. Exp. Med 212, 991–999. 10.1084/jem.20142290. [PubMed: 26077718]
38. Louveau A, Smirnov I, Keyes TJ, Eccles JD, Rouhani SJ, Peske JD, Derecki NC, Castle D, Mandell JW, Lee KS, et al. (2015). Structural and functional features of central nervous system lymphatic vessels. Nature 523, 337–341. 10.1038/nature14432. [PubMed: 26030524]
39. Munk AS, Wang W, Bèchet NB, Eltanahy AM, Cheng AX, Sigurdsson B, Benraiss A, Mäe MA, Kress BT, Kelley DH, et al. (2019). PDGF-B Is Required for Development of the Glymphatic System. Cell Rep. 26, 2955–2969.e3. 10.1016/j.celrep.2019.02.050. [PubMed: 30865886]
40. Mu R, Kim BJ, Paco C, Del Rosario Y, Courtney HS, and Doran KS (2014). Identification of a group B streptococcal fibronectin binding protein, SfbA, that contributes to invasion of brain endothelium and development of meningitis. Infect Immun 82, 2276–2286. 10.1128/iai.01559-13. [PubMed: 24643538]

Highlights:

- Identifies molecular mechanisms of meninges arachnoid barrier cell development
- Absence of arachnoid barrier cell development causes leakage into CNS
- Arachnoid barrier functionality first appears in prenatal CNS
- Appearance of barrier properties coincides with junctional protein localization

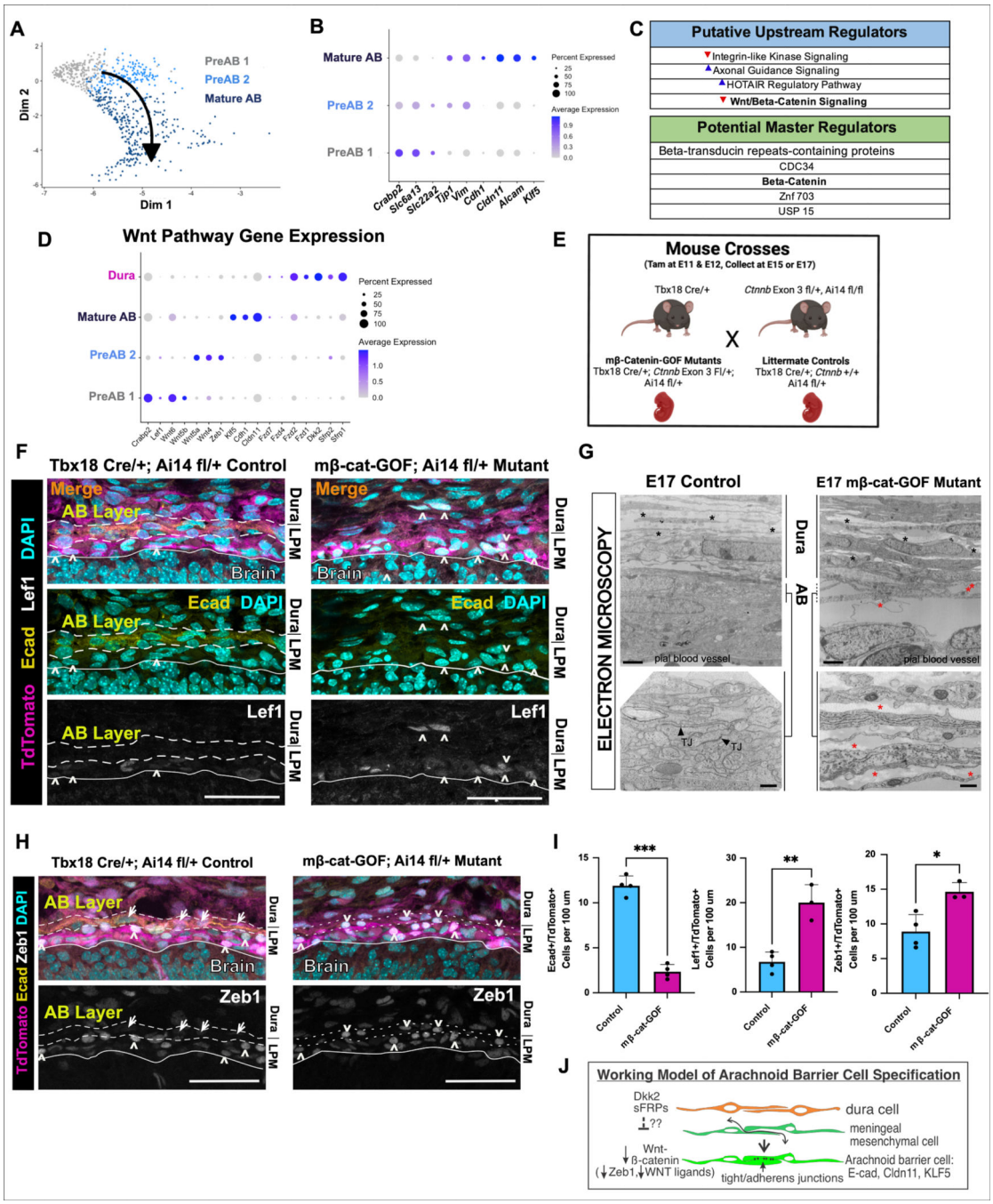

Figure 1. Downregulation of Wnt-β-catenin signaling is required for proper specification of arachnoid barrier cells.

(A) UMAP plot of E14 meningeal fibroblast subclusters PreAB1, PreAB2 and Mature AB with arrow depicting the pseudotime lineage. (B) Dotplot depiciting selected gene expression in PreAB1, PreAB2 and Mature AB clusters. (C) Ingenuity Pathway Analysis results from comparing differentially expressed genes of PreAB1 and PreAB2 vs. Mature arachnoid barrier. (D) Dotplot depicting gene expression of key Wnt pathway genes in PreAB1, PreAB2 and Mature AB and dura clusters. (E) Schematic of experimental mouse crosses and resulting embryos for analysis. (F) Images depict immunofluorescence labeling

for Lef1 and E-cadherin (to mark arachnoid barrier [AB] layer cells, outlined in the control image with dashed lines in E15 dorsal forebrain meninges. Carets indicate Lef1+/tdTomato+ cells, tdTomato labels recombined cells and DAPI labels nuclei. (G) Electron microscopy images at 4800x magnification (top) and 23,000x (bottom) from E17 control and mβ-cat-GOF mutants upper meninges. Black asterisks indicate collagen fibrils in dura cell layer and red asterisks indicate ectopic collagen fibrils. 'TJ' with arrows indicates electron dense tight junctions between arachnoid barrier cells. (H) Images depict immunofluorescent labeling for Zeb1 and E-cadherin (which marks AB layer in control) in E15 dorsal forebrain meninges. Carets indicate E-cadherin-/tdTomato+/Zeb1+ cells and arrows indicate E-cadherin+/tdTomato+/Zeb1- cells, in control these are within the AB layer (dashed lines). Dotted line in mβ-cat-GOF mutant image indicates area with many E-cadherin-/tdTomato+/Zeb1+. (I) Quantification of E-cadherin+/TdTomato+ arachnoid barrier cells, Lef1+/TdTomato+ cells, and Zeb1+/TdTomato+. (J) Working model of arachnoid barrier cell specification. Statistics: Students T-Tests, n=4 (E15 control) and 3 (E15 mβ-cat-GOF mutant) (*** = $p < 0.01$, *** = $p < 0.001$. Scale bars =250 μm in 50 μm in (F) and (H) and, 2 μm (G top) 500 nm in (G, bottom). Graphics in Figure 1E created with BioRender.com.

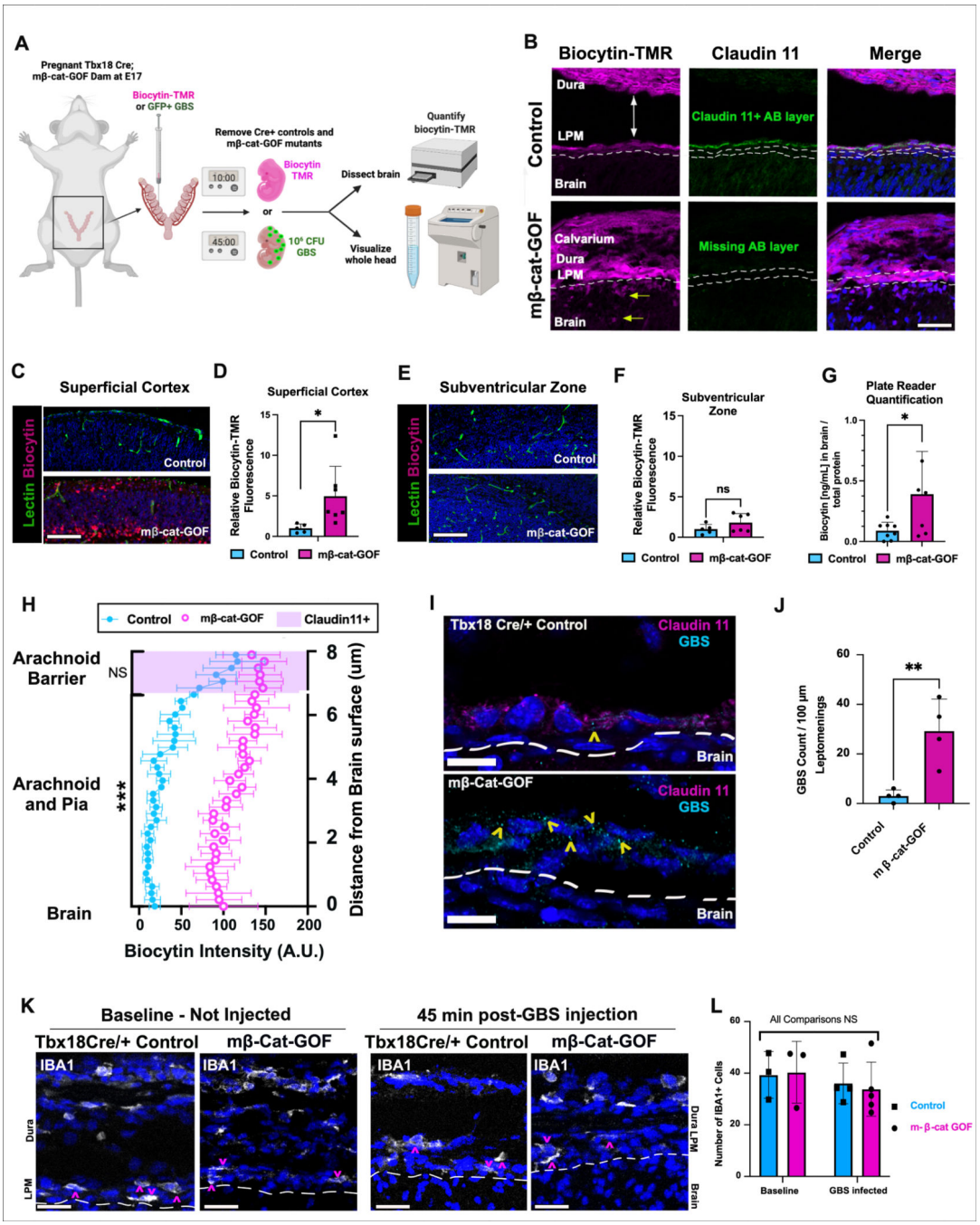

Figure 2. The fetal arachnoid barrier can prevent peripherally injected molecules and pathogens from entering the CNS.

(A) Schematic of prenatal barrier assay experiment workflow. (B) Images depict tissue sections imaged in the dorsal forebrain meninges of E17 control and mβ-cat-GOF mutants collected 10 min following peripheral Bioctyin-TMR injections, immunolabeling for Claudin 11 (marker of arachnoid barrier cells). Yellow single-headed arrows indicate tracer-labeled cells in the mβ-cat-GOF mutant brain. White double-headed arrow indicates where the leptomeninges and dura (attached to the calvarium) separate in the control during issue processing. The position of AB layer, 6.5–8 microns above the surface of

the brain, is marked by dotted white lines, where the bottom dotted line marks the bottom the leptomeninges (LPM). In mβ-cat-GOF mutants, Claudin11+ cells are missing, thus the same region of 6.5–8 microns above the brain was used for quantifying tracer entry into leptomeninges. (C) Images show Biocytin-TMR tracer present in the superficial cortex (50 microns and less from pial surface) of mutant tissue sections but not control. Lectin marks blood vessels. (D) Quantification of Biocytin-TMR fluorescence intensity from images of superficial cortex, n=6 each condition. (E) Images show no Biocytin-TMR dye is present in the deep areas of the cortex (subventricular zone) of either control or mutant tissue. Tissue stained with Lectin to mark blood vessels. (F) Quantification of Biocytin-TMR fluorescence intensity in subventricular zone regions; n=6 each condition. (G) Plate reader quantitation of Biocytin-TMR dye in superficial cortex, normalized to total protein; n=5–6 each condition. (H) Line analysis of Biocytin-TMR signal intensity in E17 control and mβ-cat-GOF leptomeninges (Claudin 11+ is shaded pink to indicate where Claudin11+ arachnoid barrier cells are in the control animals) and descending 8 microns from arachnoid barrier cells, through the arachnoid and pia, ending at brain surface; n=3, control and n=5, mβ-cat-GOF. (I) Images of dorsal forebrain meninges tissue sections from control and mβ-cat-GOF infected with GBS-GFP, sections immunolabeled for Claudin 11. Yellow carrots point to GFP+ GBS puncta in the leptomeninges. (J) Quantification of GBS burden in dorsal leptomeninges; n=4 both conditions. (K) Images of IBA1 immunolabeling in E17 dorsal forebrain meninges to identify macrophages (carets) in control and mβ-cat-GOF, baseline, uninjected and following GBS infection. (L) Quantification of IBA+ cells within meninges of control and mutant baseline, uninjected (n=3, both conditions) and GBS-infected (n=4 control and n=5 mβ-cat-GOF). Statistics: Students T-Tests for 2D, 2F, 2G, 2H, and 2J, with average of all arachnoid and pia intensity values collapsed into one value for 2H, 2-way ANOVA for 2L with multiple comparisons and Tukey Correction, * = $p < 0.05$, ** = $p < 0.01$, *** = $p < 0.001$. Dotted line marks bottom of leptomeninges in I and K. Scale bars =50 μm in B, C, E and 20 μm in I and K. Graphic in Figure 2A created with BioRender.com.

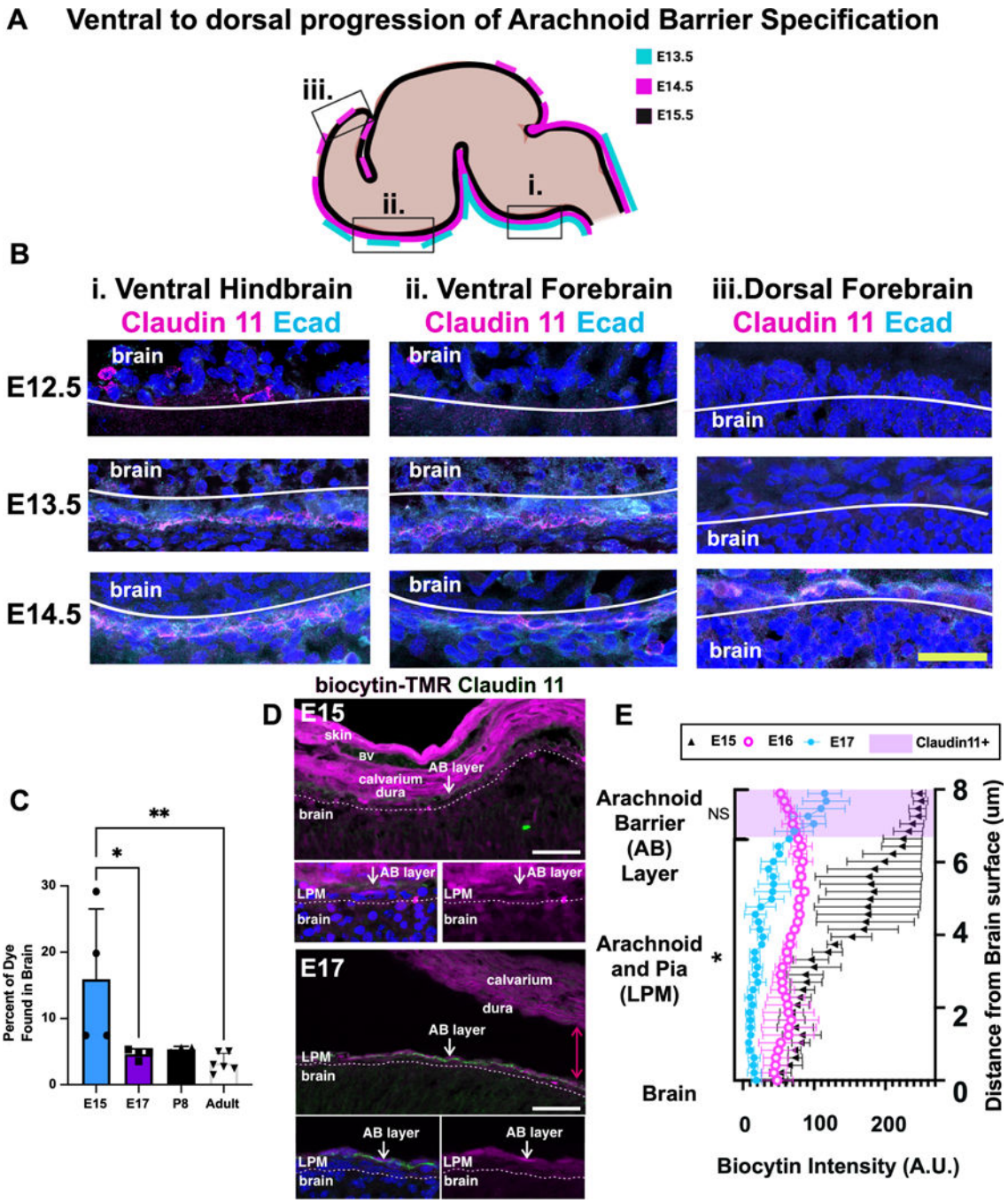

Figure 3. Arachnoid barrier cells have a ventral to dorsal wave of specification from E13-E15, which precedes barrier formation by E17.

(A) Schematic of embryonic murine brain at different ages, showing when Claudin 11 and E-cadherin expression are either patchy (dashed line) or contiguous (solid line) around the brain. Boxes drawn over the i. Ventral Hindbrain, ii. Ventral Forebrain, and iii. Dorsal Forebrain depict location where images in B were taken. (B) Images of sections with Claudin11 (magenta) and E-cadherin (cyan) immunolabeling from brain locations indicated in A, showing progressing appearance of arachnoid barrier cells from E12-E15. (C) Quantification of Biocytin-TMR barrier assay in brains from multiple ages; n=4 (E15, E17,

P8) n=5 adult. (D) Images show dorsal forebrain sections from E15 and E17 Biocytin-TMR injected embryos with Claudin 11 immunolabeling to mark arachnoid barrier (AB) cell layer. (E) Quantification of Biocytin-TMR fluorescence signal within the leptomeninges using tissue sections from E15 vs. E16 vs. E17 embryos, n=3 each age. Two-way Students T-Tests for 3C and 3E, with average of all arachnoid barrier or arachnoid and pia intensity values collapsed into one value for 3E, and a significant difference between E15 and both E16 and E17, but no significant differences between E16 and E17, * = $p < 0.05$, ** = $p < 0.01$, *** = $p < 0.001$. Scale bars = 50 μm in B and D.

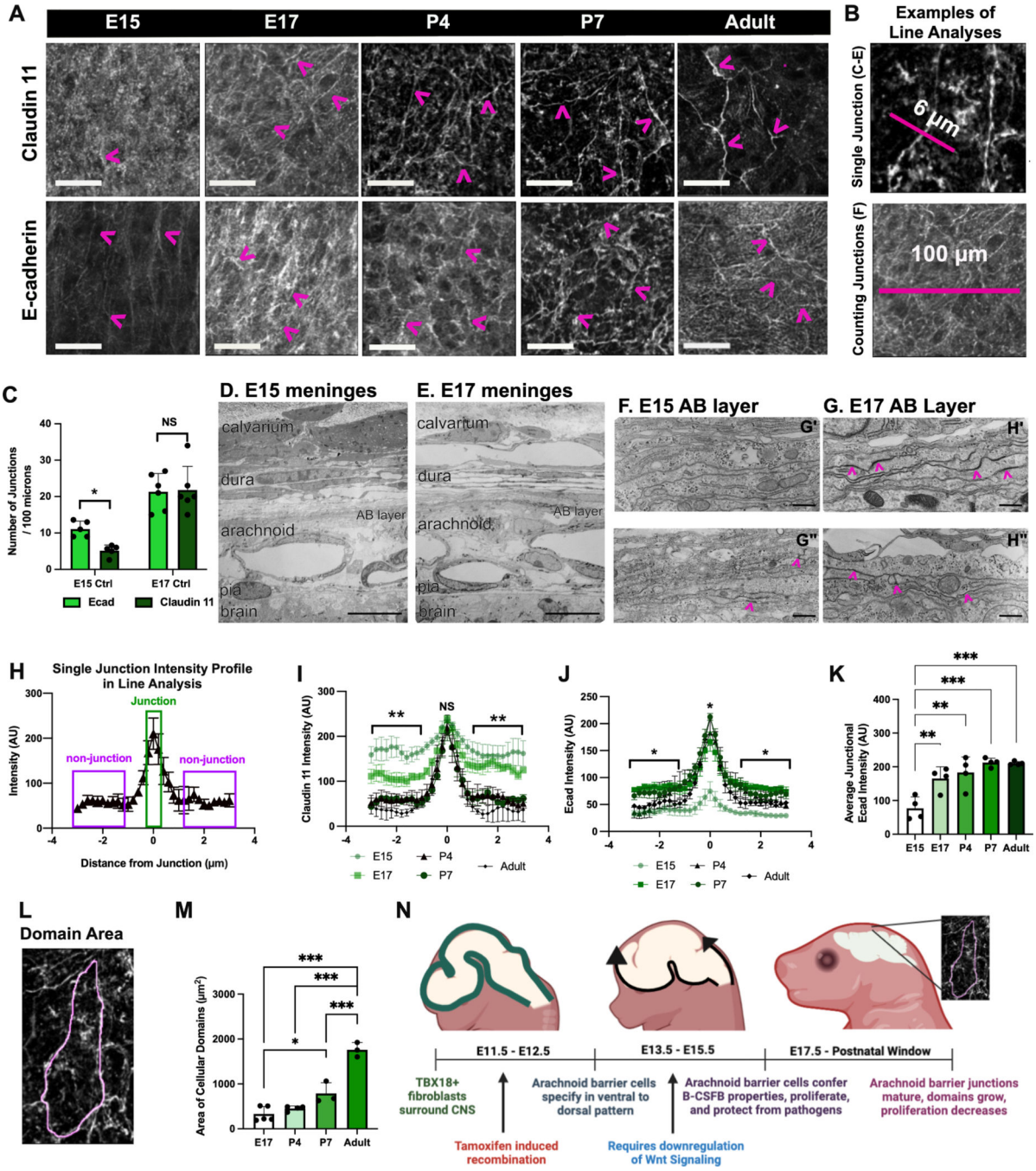

Figure 4. Prenatal emergence of arachnoid barrier tight and adherens junctions that mature postnatally.

(A) Images of cerebral leptomeninges whole mounts harvested from wildtype animals at E15, E17, P4, P7, and adult ages immunolabled for Claudin 11 (top row) or E-cadherin (bottom row) expression. Carets indicate cell-cell junctions. (B) Top images demonstrates quantification method used to measure fluorescent intensity profile of individual junctions in 4H-J and bottom image demonstrates quantification methods used to count the number of junctions per 100 µm in 4C (bottom). (C) Number of junctions found in E15 and E17 leptomeningeal whole mounts per 100 µm, as defined by a peak that is >50 florescence AU

higher than the fluorescence values 1–2 μm away for E-cadherin and Claudin 11; n=5, E15 and E17. (D, E) 1900x magnification electron microscopy images of E15 and E17 meninges. (F, G) 23,000x images of E15 and E17 arachnoid barrier (AB) layers region. Carets point to electron dense tight junctions. (H) Chart demonstrates single junction intensity profile analysis method, where non-junctional intensity was quantified as 1–3 μm away from the junction on either side and junctional intensity was quantified as the central peak. (I) Quantification of Claudin11+ single junction line intensity profile from E15 to adult; n=4, all ages. (J) Quantification of E-cadherin+ single junction line intensity profile from E15 to adult; n=4, all ages. (K) Average junction intensity of E-cadherin from E15 to Adult, n=4, all ages. (L) Example of how a single domain area was defined for purposes of analysis. (M) Graph depicts Claudin11+ domains size from E17 to Adult; n=5 (E17), n=4 (P7), n=3 (P7 and adult). (N) Schematic showing developmental timeline of arachnoid barrier specification and maturation. Statistics: Students T-Tests for 4C, 4I, 4J, and 4M (all non-junctional values collapsed into 1 value for 4I and 4J) and Two-way ANOVA with multiple comparisons and Tukey correction for 4K and 4M. * = $p < 0.05$, ** = $p < 0.01$, *** = $p < 0.001$. Scale bar = 50 μm in 4A, 10 μm in 4D and 4E, 500 nm in 4F and 4G. Graphic in 4N created in BioRender.com.

KEY RESOURCES TABLE

REAGENT or RESOURCE	SOURCE	IDENTIFIER
Antibodies		
Rabbit polyclonal anti-S100A6	Novus Biologicals	Cat#: NBP1–89388
Mouse monoclonal anti-CRABP2	Millipore	Cat#: MAB5488
Rabbit polyclonal anti-RALDH2	Sigma-Aldrich	Cat#: HPA010022
Chicken polyclonal anti-GFP	Invitrogen	Cat#: A10262
Mouse monoclonal anti-E-Cadherin	BD Transduction	Cat#: 610181
Rat monoclonal anti-Ctip2	Abcam	Cat#: ab1846
Rabbit polyclonal anti-Desmin	Cell Signaling	Cat#: 5332S
Rabbit polyclonal anti-Lef1	Cell Signaling	Cat#: 2230S
Rabbit polyclonal anti-Zeb1	Cell Signaling	Cat#: 70512
Rabbit polyclonal anti-Claudin 11	Thermofisher	Cat#: PIPA568608
Lectin	Vector	DL-1178
Rabbit anti-KLF5	Genetex	GTX103289
Rabbit polyclonal anti-IBA1	Wako	Cat#: 01919741
eBioscience Fixable Viability Dye eFluor 506	Thermofisher	Cat#: 65–0866-18
F4/80-BV785	Biolegend	Cat#: 123141
Ultra-LEAF Purified CD16/32	Biolegend	Cat#: 1330
CD45-BUV395	BD Biosciences	Cat#: 564279
CD11b-FITC	Thermofisher	Cat#: 11–0112-41
Ly6G-APC	Thermofisher	Cat#: 17–9668-82
Critical Commercial Assays		
Click-it EdU Assay – AlexaFluor 647	Termofisher	Cat#: C10635
Biocytin TMR	Thermofisher	Cat#: T12921
Experimental Models: Organisms/Strains		
Mouse: Tbx18$^{tm3.1(cre/ERT2)Sev}$/J	The Jackson Laboratory	Stock No: 031520
Mouse: Ctnnb1^{tm1Mmt}	Harada et al., 1999[22]	NA
Mouse: B6.Cg-*Gt(ROSA)26Sor*$^{tm14(CAG-tdTomato)Hze}$/J	The Jackson Laboratory	Stock No: 007914
Mouse: C57Blk/6J	The Jackson Laboratory	Stock No: 000664
GBS: COH1+pDESTerm-GFP	Mu et al., 2014[44]	NA
Software and Algorithms		
R (3.6.3), R(3.6.1)	R Foundation for Statistical Computing	https://cran.r-project.org/
Seurat (3.1.1)	Butler et al., Nature Biotechnology 2018; Stuart*, Butler*, et al., Cell 2019.	http://satijalab.org/seurat/
Ingenuity Pathway Analysis (IPA) (September 2019 Release)	QIAGEN	Cat#: 830018
FIJI	Distribution of ImageJ	https://imagej.net/software/fiji/downloads
ggplot2	R Studio	https://ggplot2.tidyverse.org/

REAGENT or RESOURCE	SOURCE	IDENTIFIER
GraphPad Prism	GraphPad Software Inc	https://www.graphpad.com/scientific-software/prism/